# Design of a flying demonstrator wing for manoeuvre load alleviation with cruise shape constraint

Sodja, Jurij; Werter, Noud P.M.; De Breuker, Roeland

**DOI**
10.2514/6.2018-2153

**Publication date**
2018

**Document Version**
Accepted author manuscript

**Published in**
AIAA/ASCE/AHS/ASC Structures, Structural Dynamics, and Materials

# Design of a flying demonstrator wing for manoeuvre load alleviation with cruise shape constraint

Jurij Sodja*, Noud P. M. Werter† and Roeland De Breuker‡
*Delft University of Technology, The Netherlands*

**Application of the aeroelastic framework developed at Delft University of Technology to a design of the tailored composite wing for a flying demonstrator is presented in this paper. In the design process the structural mass of the wing is minimised including a cruise shape constraint. Introduction of the cruise shape constraint is explained as well as a number of other important design requirements which were imposed in order to obtain a feasible and flight worthy design. The effect of the cruise shape constraint is investigated by performing a comparison study. For this purpose two wing types were defined: the reference wing and the tailored wing. The difference between the two wings is in the laminate definition comprising each wing. The reference wing was designed with symmetric-balanced laminates, while symmetric-only laminates were used for the tailored wing. The comparison was performed in terms of laminate stiffness and thickness distribution along the span, jig twist, and the aeroelastic response. Elastic deformations, aerodynamic load distribution and wing root loads are compared within the scope of aeroelastic response.**

## I. Introduction

AEROELASTIC tailoring has been researched extensively over the years. A summary of early research on aeroelastic tailoring of swept and unswept wings has been written by Shirk et al.[1] More recently Qin et al.[2,3] have done research on assessing the aeroelastic instability of composite thin-walled beams to investigate the effect of aeroelastic tailoring. Furthermore, several papers on the use of aeroelastic tailoring in general and the potential benefits it has, have been written recently by Weisshaar.[4–7] More specific research on the use of aeroelastic tailoring has been done to minimize structural weight,[8–12] maximize flutter speed[10,11,13–16] optimise the gust response characteristics of wings,[17,18] and the effect of tow-steered composites on wing aeroelastic characteristics.[19] An example of the use of aeroelastic tailoring in non-aerospace applications is the research by Thuwis et al.[20] on the use of aeroelastic tailoring on the rear wing of a F1 car.

In addition to several numerical studies, a number of experiments have been performed on tailored composite plates in order to assess divergence and flutter characteristics of such structures.[21–25] These experiments have been performed on plate-like structures hence they are unsuitable for validation of aeroelastic design frameworks dealing with wing structures having a closed-cell cross section. Wind tunnel experiments involving such tailored composite wings with a closed-cell cross section have been presented only recently by Werter et al.,[26] and Sodja et al.[27]

Evidently, substantial theoretical and experimental research has been already performed. Nevertheless, experimental data obtained in a real-life environment, outside the laboratory, which can be used for the assessment of the benefits of aeroelastic tailoring on manoeuvre load alleviation and for the validation of aeroelastic design frameworks are still missing. Therefore, the objective of this paper is to present and compare the preliminary design of a tailored composite wing to a reference wing design which will be tested using a flying demonstrator within the FLEXOP (Flutter Free FLight Envelope eXpansion for ecOnomical Performance improvement) project. Both wings are optimised with the same design requirements including

*Senior scientist, Faculty of Aerospace Engineering, Aerospace Structures and Computational Mechanics, Kluyverweg 1, 2629 HS Delft; J.Sodja@tudelft.nl

†Faculty of Aerospace Engineering, Aerospace Structures and Computational Mechanics, Kluyverweg 1, 2629 HS, Delft; N.P.M.Werter@tudelft.nl

‡Associate Professor, Faculty of Aerospace Engineering, Aerospace Structures and Computational Mechanics, Kluyverweg 1, 2629 HS Delft; R.deBreuker@tudelft.nl

having the same cruise shape ensuring that both wings have the same aerodynamic performance at cruise conditions. The only difference in the design requirements between the two wings is the laminate definition. Symmetric-only laminates are used for the tailored wing, while symmetric-balanced laminates are used for the reference wing.

This paper is organised as follows. First the aeroelastic framework used to perform the design studies is briefly introduced in Sec. II. Introduction of the cruise shape as a design constraint is explained in Sec. III followed by an explanation of the other design requirements in Sec. IV. Finally, the obtained results are discussed in Sec. V followed by the conclusions in Sec. VI.

## II. Aeroelastic design framework

An aeroelastic analysis and design framework was developed at the Delft University of Technology to improve the conceptual design of aircraft wings by including aeroelastic effects. The aeroelastic design framework has to be computationally efficient to be able to perform design optimisation studies quickly. For this purpose, the three-dimensional wing geometry is reduced to a 1D Timoshenko beam model. The resulting beam model is split in several spanwise sections, each having its own skin laminate distribution throughout the wing cross-section. These laminates are described using lamination parameters and the laminate thickness. Consequently any laminate is fully defined by a fixed number of continuous design variables, allowing for the use of efficient, gradient-based optimisers. A detailed explanation of the aeroelastic design framework is given by Werter and De Breuker.[28]

The aeroelastic analysis and optimisation loop is depicted in Fig. 1. the loop starts with the definition of the wing geometry and load cases as inputs. Next, the composite laminate properties used for the wing skins and spars are determined based on the material properties given as input and the lamination parameters and thicknesses generated by the optimiser. The beam model is generated by performing the cross-sectional analysis on the cross-sectional geometry accounting for the laminate properties. Therewith the Timoshenko cross-sectional stiffness matrix with respect to the beam reference axis is generated. A detailed explanation of the cross-sectional analysis is given by Ferede and Abdalla.[29]

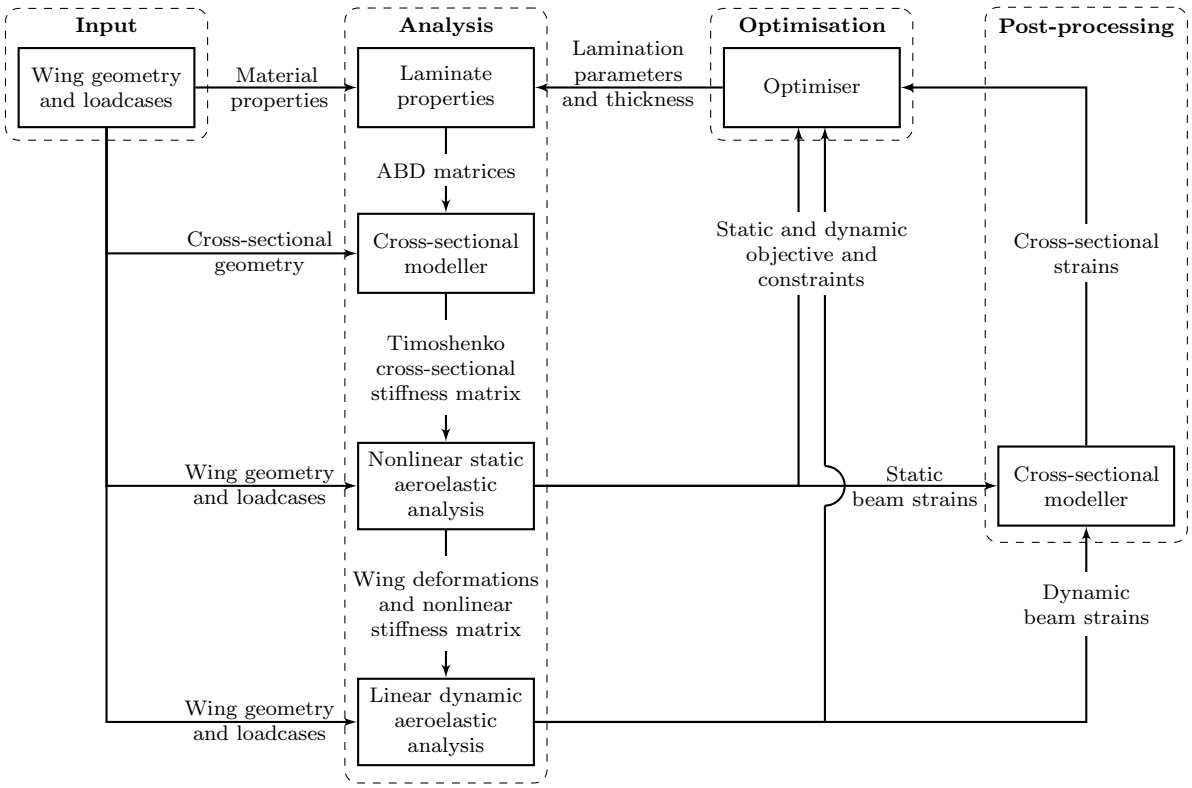


**Figure 1. Schematic representation of the aeroelastic analysis and optimisation loop[28]**

As a third step, a geometrically nonlinear static aeroelastic analysis for each load case is carried out. The static aeroelastic analysis closely couples a geometrically nonlinear Timoshenko beam model based on the co-rotational formulation and a vortex lattice aerodynamic model. A geometrically nonlinear aeroelastic solution is obtained by using load control and the Newton-Raphson root finding method. A geometrically nonlinear model is used to account for large deformation due to applied loads and enforcement of the cruise shape constraint via morphing of the wing's unloaded shape. The selected structural and aerodynamic model ensure a computationally efficient model suitable for optimization.

In order to account for the effects of gravity due to structural and non-structural masses and engine thrust, the model includes also eccentric follower and non-follower forces based on the same co-rotational formulation already used for the structural model.

As a final analysis step, a linear dynamic aeroelastic analysis is carried out around the nonlinear static equilibrium solution. The nonlinear structural stiffness matrix, obtained from the static analysis is linearised and coupled to a linear mass matrix to obtain the dynamic structural model. This model is then coupled to an unsteady aerodynamic model based on the unsteady vortex lattice method.[30] Using the linear dynamic analysis, the flutter and divergence speed are calculated, and dynamic displacements can be obtained under e.g. gust loads.

The strains in the three-dimensional wing structure are retrieved in a post-processing step by using the cross-sectional modeller to convert the beam strains and curvatures to the skin strains. This allows for evaluation of various structural constraints such as maximum allowable strain and buckling which are also included in the optimisation process.

Finally the static and dynamic responses, and the skin strains are then fed into the optimiser as objective or constraint and a gradient based optimiser is used to update the set of lamination parameters and thickness until a converged solution is found.

## III. Cruise shape constraint

Cruise shape as a design requirement was selected due to the fact that the wing shape in cruise condition is driven mainly by the aerodynamic performance requirements rather than structural efficiency considerations. By enforcing this constraint the aerodynamic performance of the wing is not compromised by aeroelastic tailoring aimed at structural mass minimisation or passive load alleviation.

A cruise shape constraint is imposed on the total spanwise twist distribution of the wing at 1g cruise conditions which is a sum of the geometrical twist distribution initially built into the wing's jig shape and the elastic twist deformation due to the applied external loads (e.g. aerodynamic forces, engine thrust or weight due to non-structural mass). Other requirements, such as wing dihedral and the amount of out-of-plane deformation were neglected since their influence on the load distribution over the wing and on the aerodynamic performance of the wing is negligible.

Whether or not the optimiser is able to meet the cruise shape constraint by aeroelastic tailoring alone depends on the combination of the prescribed jig shape of the wing, other enforced constraints and the selected design load cases. Furthermore, the question is whether any load alleviation can be achieved in addition to meeting the cruise shape constraint. Hence it is necessary to include the wing jig shape in the optimisation process as a design variable. Spanwise twist distribution pertinent to the jig shape is thus treated as a set of morphing design variables which control the wing twist as shown in Fig. 2. This way the optimiser is given additional freedom to trade-off between tailoring the laminate stiffness and thickness, and adjusting the jig twist of the wing in order to arrive at the most optimum wing design. Details about the implementation of the jig twist as a morphing variable in the aeroelastic framework can be found in the works by De Breuker et al.,[31] Werter et al.[32] and Werter.[33]

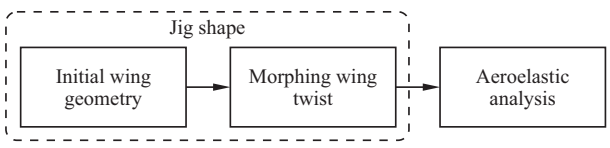


**Figure 2. Jig shape introduced as a morphing parameter in aeroelastic analysis[33]**

The final jig shape is recovered at the end of the optimisation process by applying the morphing twist

to the initial wing geometry at the absence of any external loads. The cruise shape was enforced with a margin of $\pm 0.05$ deg which results in a jagged spanwise twist line which pivots between the upper and lower bounds as shown by the red line in Fig. 3a. These oscillations also propagate to the recovered jig shape shown by the blue line in Fig. 3b. Hence it was decided to introduce two additional post-processing steps in the jig twist recovery. First, the difference between the resulting, optimised 1g flight twist and the required reference twist was obtained and subtracted from the raw recovered jig shape depicted by the green symbols in Fig. 3b. The corrected jig twist along the span has clearly improved. Most of the jagged corners have been removed. Nevertheless, small oscillations can still be observed. Thus, a smooth spline has been fitted to the corrected jig twist in order to obtain the final jig twist depicted by the red line in Fig. 3b. The same procedure was applied to all the studies shown in this paper.

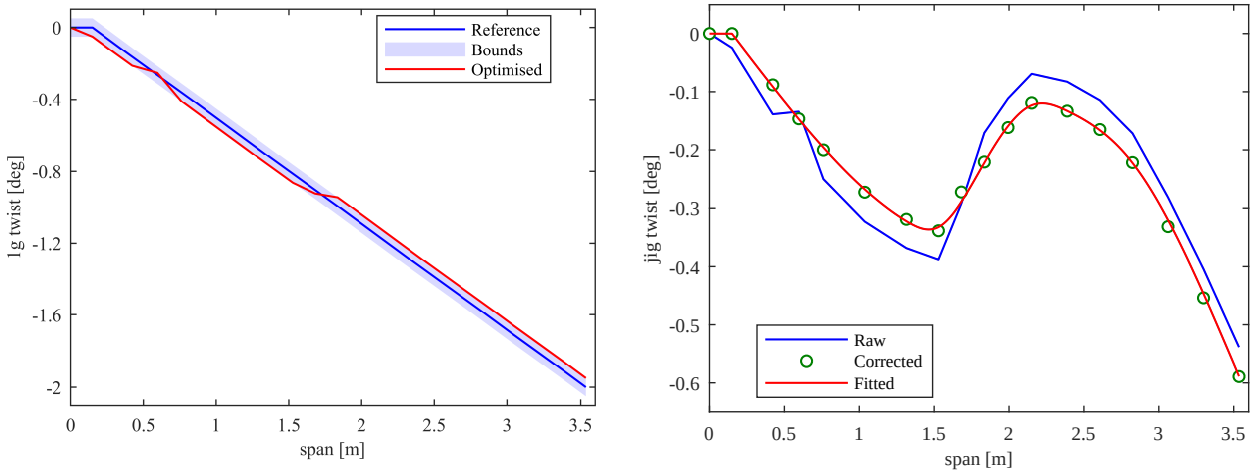


(a) 1g flight shape

(b) Jig shape

**Figure 3. Jig shape recovery**

## IV. Design setup

In order to obtain a wing design which is flight worthy and resembles the final wing as closely as possible a number of design requirements in addition to the cruise shape constraint have been applied. Among others, planform properties, structural layout, laminate properties, operating conditions, safety requirements, control surfaces, and design regions. Planform properties and structural layout are summarised in Fig. 4 and Table 1. The wing thickness is linearly decreasing from 10% chord to 8% chord from root to tip.

**Table 1. Wing geometry**

| Parameter | Value |
|---|---|
| Semi-span | 3.536 m |
| Chord, root | 0.471 m |
| Chord, tip | 0.236 m |
| Thickness, root | 10% chord |
| Thickness, tip | 8% chord |
| Sweep, leading edge | 20 deg |

The structural layout is chosen in the form of a wingbox, whereas the leading edge part is excluded from the structural design as part of the load carrying structure since it acts only as an aerodynamic fairing. Nevertheless, the area of the leading edge should be kept as small as possible to minimise its effect on the overall aeroelastic response of the wing. The wingbox will also have to house the control surface actuators and instrumentation, such as fibre Bragg and acceleration sensors to monitor the wing deformation and motion.

Finally, the wingbox should represent the size of a conventional wing box used in a typical commercial aircraft. Therefore the maximum possible size of the wingbox was chosen. The front spar was located at 15% chord and the rear spar was located at 71% chord.

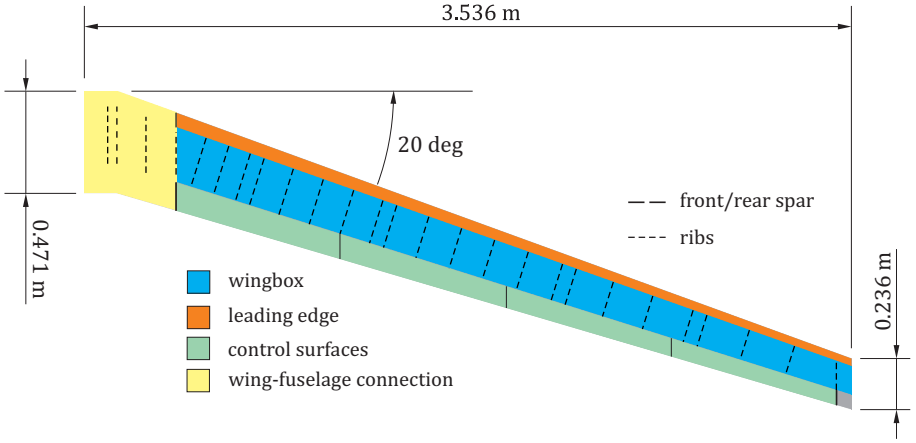


**Figure 4. Wing structural layout**

The rib distribution as shown in Fig. 4 is governed by three factors: a.) unified wing-fuselage interface, b.) unified control surface and actuator layout across the considered wings, and c.) by the buckling behaviour of the load bearing skins. A unified wing-fuselage interface, and control surface layout is required for integration of the designed wings with the rest of the flying demonstrator. The rib pitch affects the buckling behaviour of the wingbox by breaking the load bearing skins into smaller panels. Typically the smaller the panel the larger the buckling load it can support at given thickness and stiffness properties. Hence it was decided to cluster the ribs closer together at the root of the wing where the in-plane loads are the higher and spread them further apart towards the tip of the wing. The ribs also provide support to the control surface actuators. Therefore, each actuator was enclosed by two ribs, which can be observed in Fig. 4 by an irregular pattern in the rib spacing and two ribs position close to each other.

A standard carbon-fibre-epoxy unidirectional prepreg $C8552S/34\%/UD134/AS4$ was chosen for wing manufacturing due to material's good tailoring capabilities, and availability. Furthermore, the use of unidirectional prepreg allows for accurate reproduction of ply angles during the laminate assembly in the forming tool.

Standard ply stacks used in commercial aircraft can be approximated by a $[0_{60\%}/\pm 45_{30\%}/90_{10\%}]_S$ stack. Such laminates can be accurately represented if the cured ply thickness relative to the total laminate thickness is very small. In the case of the considered wings it is expected that the ply number comprising the laminate will be at an order of 10, hence it would be impossible to maintain or remain close to the afore mentioned ply representation in the laminate upon casting the optimised laminate stiffness and thickness distribution into an actual, producible stacking sequence. Therefore, it was decided to constrain the layup comprising the reference wing to symmetric and balanced ply stacks. The tailored wing, on the other hand is only constrained to symmetric ply stacks.

Balanced-symmetric laminates are sensitive to the definition of the reference material axis which defines the 0 deg ply orientation as illustrated in Fig. 5. Due to the manufacturing requirements the 0 deg plies had to be aligned with one of the spars. Hence it was decided to choose the rear spar as the reference material axis, since it was found out that it yielded larger mass reduction for the balanced-symmetric laminate comprising the reference wing.

Positive and negative limit loads used in the design process are set at 5g and -2g respectively. Positive and negative limit loads are set to different load factors due to the manner in which the airplane will be operated during testing. In order to demonstrate load alleviation only manoeuvres with positive load factor are foreseen, whereas manoeuvres with negative load factors are to be avoided. In addition, due to the asymmetric shape of the selected airfoil it is expected that the aircraft cannot achieve negative loads as high as positive.

Safety requirements are imposed in terms of a prescribed safety factor and in terms of knock down factors applied to the material allowables. The safety factor is set at 1.5. This way sufficient margin between the

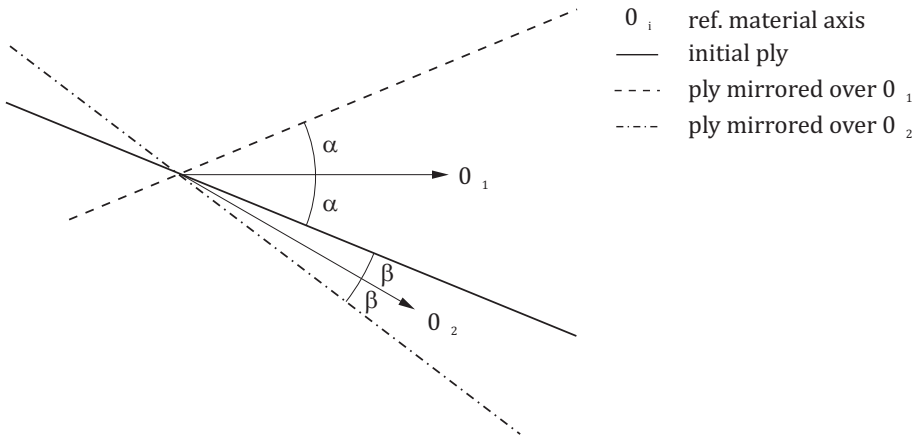


**Figure 5. The effect of reference material axis on a balanced laminate**

limit and the ultimate load is guaranteed.

Both strength and stiffness properties of composites are well known to be susceptible to manufacturing inaccuracies, environmental changes and damage during part manufacturing and service life.[34] Hence the actual individual property values can depart significantly from the nominal values provided by the material manufacturer. In order to ensure structural strength of the designed wings, it was decided to use the B-basis knockdown for the material scatter, the 90 deg/wet knockdown for the environmental effects and the knockdown for the barely visible damage that might occur during service.

Stiffness properties used in the calculation of the aeroelastic response were not subjected to any knockdown factors and the mean stiffness values were used directly. However, a B-basis knockdown was applied to the stiffness properties in the evaluation of the critical buckling load in order to provide sufficient margin of safety.

The control surface layout is shown in Fig 4. Control effectiveness was added as a design constraint in order to ensure that the controls have sufficient authority throughout the entire flight envelope. Control effectiveness, $\eta_{ail}$) is defined by Eq. 1 as a negative ratio between the roll coefficient due to control surface deflection, $C_{L\delta}$ and the roll coefficient due to roll damping $C_{Lp}$.

$$\eta_{ail} = -C_{L\delta}/C_{Lp} \tag{1}$$

The minimum acceptable control effectiveness was set to 0.15, which at a 10 deg aileron deflection in cruise and landing conditions corresponds to a roll rate of 19.2 deg/s and 8.2 deg/s respectively. Aileron deflection assumes that all three ailerons are deflected the same amount in antisymmetric fashion on starboard and port side of the main wing.

Finally, the laminate comprising the wing is optimised in spanwise constant patches called design regions. Within each design region a set of lamination parameters and laminate thickness are optimised with an objective to reduce the overall structural mass of the wing. The wing is split in $12 \times 1$ spanwise and chordwise design regions along the span as shown in Fig. 6. Chordwise number of design regions is restricted to 1 due to the manufacturing limitations.

## V. Results

Comparison between the reference and the tailored wing is presented in this section. First, design parameters such as weight, thickness, jig twist and stiffness distribution are compared, followed by a comparison of the aeroelastic response at the selected design load cases. Aeroelastic response is analysed in terms of wing deformation, aerodynamic properties, and root loads. In addition important design constraints are also discussed within the scope of aeroelastic response.

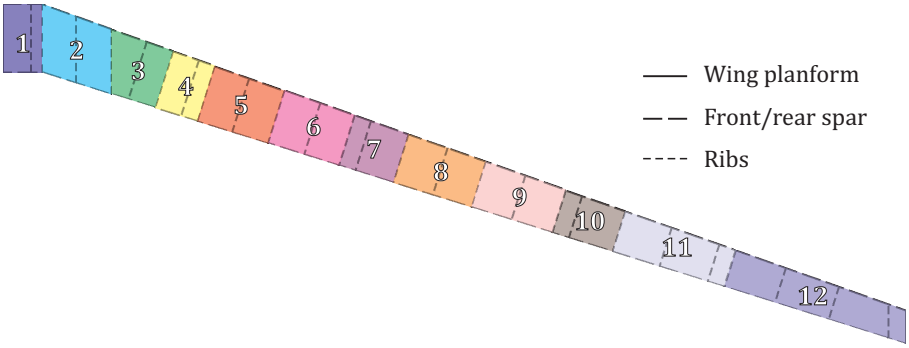


**Figure 6. Design region distribution**

### A. Design parameters

The thickness distributions of the laminates comprising the top skin, bottom skin, and the spars are compared in Fig. 7. Similar thickness behaviour in the top and bottom skin can be observed for both wings. Similar trends result from, on one hand, identical structural layout of the spars and ribs, and, on the other hand, from the fact that both wing designs are driven by the same constraint type, namely buckling. Moreover, the optimised bottom skin is thinner relative to the top skin due to the less sever maximum negative load case in comparison to the maximum positive load case. One can also observe that for both wing types both the front and the rear spars are of constant thickness of 1 mm which corresponds to the minimum laminate thickness constraint.

There is a noticeable difference between the reference and the tailored wing in thickness of the wingbox skins which stems from the difference in the tailoring capability of symmetric-balanced and symmetric laminates. Symmetric laminates comprising the tailored wing allow for more aggressive tailoring in order to alleviate aerodynamic loads and mitigate buckling which allows for larger structural mass reduction. The difference in laminate tailoring is illustrated in Fig 9.

Furthermore, the difference in skin thickness between the two wing types differs significantly for the top and the bottom skin. The difference in the top skin thickness is on average 0.08 mm, while there is on average 0.14 mm of difference in the bottom skin thickness. Relative difference between individual skins is also shown in Fig. 7. The difference is explained by inspecting the aeroelastic response at $-2$ g load case in conjunction with the jig twist. According to Fig. 8, the jig twist pertinent to the reference wing exhibits considerably more wash-out towards the wing tip relative to the tailored wing. As a result the outboard part of the reference wing is exposed to considerably higher aerodynamic loads in the $-2$ g load case, as shown in Fig. 13b, which translate to considerably higher root loads as reported in Table 3. Hence the thickness of the reference wing bottom skin has to be increased in order to be able to resist higher buckling loads due to larger bending moment. From the perspective of the 5 g load case, the jig twist of the reference wing is more favourable in terms of load alleviation since the wing has considerable amount of wash-out already built in its jig shape. Nevertheless, the top skin of the tailored wing is still thinner due to the better load alleviation capabilities of the symmetric laminates comprising the tailored wing. However, the difference in thickness is smaller.

Mass comparison is summarized in Table 2. Structural mass accounts only for the material mass comprising the wingbox. Total mass accounts in addition to structural mass also for all non-structural masses installed in the wing such as ribs, control surfaces, actuators, paint and sensors. It is important to point out that both structural and total mass are expressed per semi-span. Finally, the AC mass accounts for the total mass of the aircraft including the fuselage and the empennage mass.

The difference in skin thickness between the reference and the tailored wing results in a 4% structural mass reduction in favour of the tailored wing. Since the structural mass of the wing represents a fraction of the total aircraft mass the total mass reduction on the aircraft level diminishes to about 1%.

The optimised jig twist of the reference and the tailored wing is compared in Fig 8. In comparison to laminate thickness distribution the difference between the two compared wing types is more pronounced. First, the amount of jig twist required for the reference wing is, in general, much larger. In the case of the

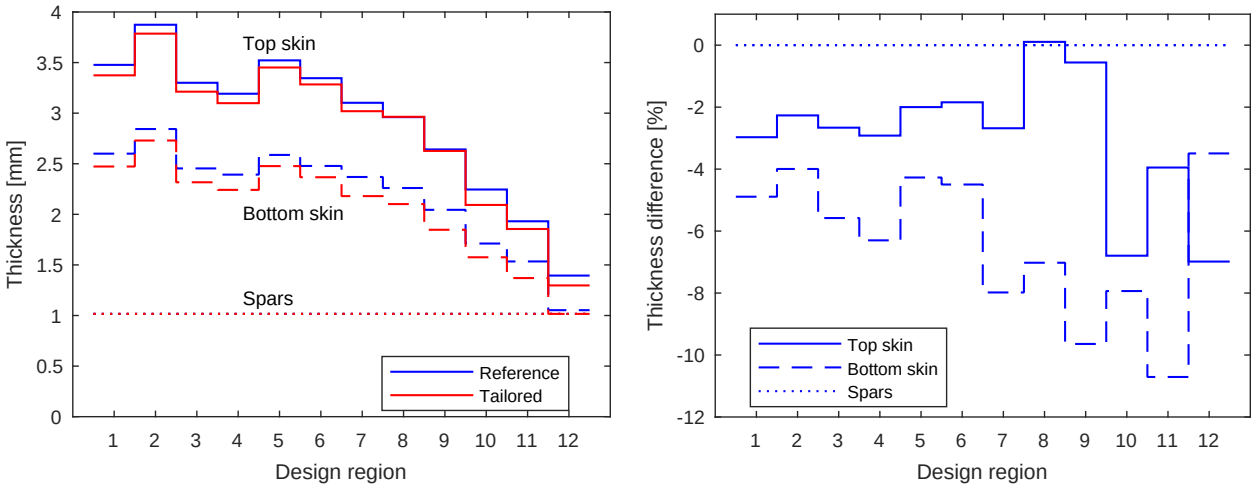


(a) Laminate thickness (b) Laminate thickness comparison

**Figure 7. Laminate thickness distribution along the wing span**

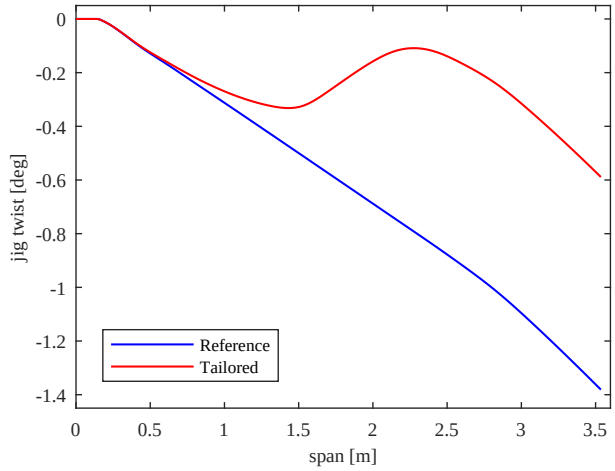


**Figure 8. Jig twist comparison**

**Table 2. Mass comparison per semi-span of the wing**

| Wing | Str. mass [kg] | Total mass [kg] | AC mass [kg] |
|---|---|---|---|
| Reference | 5.884 | 12.064 | 65.392 |
| Tailored | 5.652 (-4%)† | 12.064 (-2%) | 64.929 (-1%) |

† Relative difference with respect to the reference wing.

reference wing, the wing tip has a jig twist of $-1.38$ deg whereas the tailored wing tip has a jig twist of only $-0.59$ deg. Second, the jig twist of the reference wing monotonically decreases along the span, while the jig twist of the tailored wing exhibits non-monotonic behaviour. The observed differences are explained by the difference in the imposed laminate constraints. In comparison to the symmetric-only laminates used in the tailored wing, the symmetric-balanced laminates comprising the reference wing cannot exhibit any extension-shear or bend-twist coupling. Consequently, in the case of the reference wing, the bending moments resulting from the aerodynamic loads cannot induce any torsional deformation due to the afore mentioned material couplings. As a result, in order to meet the 1 g shape requirement more twist has to be built into the jig shape of the reference wing.

Both membrane and bending stiffness distribution along the span of the reference and the tailored wing are compared in Fig. 9. Based on the results shown in Figs. 9a and 9c, one can identify three distinct tailoring regions in the membrane stiffness of both top and bottom skin: the root, the central, and the tip part of the wing. For both, the reference and the tailored wing, prominent membrane stiffness tailoring is present in the central part of the wings only while tailoring is less evident at the root and tip part of the wing. The obtained membrane stiffness is highly anisotropic in the central part of the wing with the dominant stiffness directions oriented diagonally forward with respect to the wing reference axis going from trailing edge to the leading edge. Due to the difference in the laminate constraint between the two wing types the tailoring is much more pronounced in the case of the tailored wing. Moreover, the membrane stiffness is only weakly tailored for both wing types in the spar members of the wingbox which is indicated by a nearly circular stiffness rosettes.

Tailoring of the laminate bending stiffness is considerably more pronounced relative to the tailoring of the laminate membrane stiffness for all wingbox members and for both the reference and the tailored wing. Expectedly, the tailoring process is more prominent in the case of the tailored wing which results in stiffness rosettes which are dominated by a specific stiffness orientation. In the case of the reference wing, there always exists an equally prominent conjugate stiffness direction with respect to the defined material axis due to the balanced laminate constraint. Similar to the membrane stiffness behaviour in the top and bottom skin, one can identify three distinct tailoring regions for both of the two wing types. The tailoring process yields laminate stiffness dominated by the stiffness orientation along or slightly aft of the wing reference axis at the root of the wing. In the central part of the wing, the laminate stiffness is oriented diagonally forward with respect to the beam reference axis going from trailing edge to the leading edge. In the tip region of the wing the laminate stiffness is oriented symmetrically around the beam reference axis which also coincides with the definition of the material axis.

The observed tailoring patterns can be explained by considering the incentives raised due to the definition of the optimisation problem. As can be seen in Fig. 11 and 12, the buckling constraint is critical over most of the wing. Hence, the bending stiffness is heavily tailored in order to be able to reduce the skin thickness as much as possible and obtain the maximum possible reduction in structural mass. On the other hand, one can conclude from the strain constraint values that the wing is more than strong enough to support the aerodynamic loads in 5 g and $-2$ g load case. Hence the degree of tailoring in the membrane stiffness is rather low.

The central part of the wing is still critical in buckling. However, one can also observe a large increase in the torsional deformation of the tailored wing between 1.5 m and 2.5 m span as shown in Fig. 10b which allows the wing structure to alleviate aerodynamic loads by re-distributing them towards the inboard section of the wing. The tailoring result in the central part of the wing is thus a trade-off between satisfying the buckling constraint and promoting passive load alleviation which leads to a more distinct and prominent tailoring in both membrane and bending stiffness. It is important to point out that the membrane and bending stiffness are not independent of each other. Hence the tailoring pattern in the membrane stiffness can reflect in the tailoring pattern in the bending stiffness and vice versa.

Finally, the tip section of the wing undergoes little deformation which results in low sensitivity of the optimisation process to tailoring for load alleviation. Nevertheless, part of the tip section is still critical in buckling which explains the tailoring patterns observed in the bending stiffness.

### B. Aeroelastic response

This section presents the aeroelastic response of the reference and the tailored wing for the 1 g, 5 g, and the $-2$ g load case. First structural response is reviewed in terms of out-of-plane and torsional deformation of the wings followed by the discussion of structural constraints. Then aerodynamic characteristics such as lift

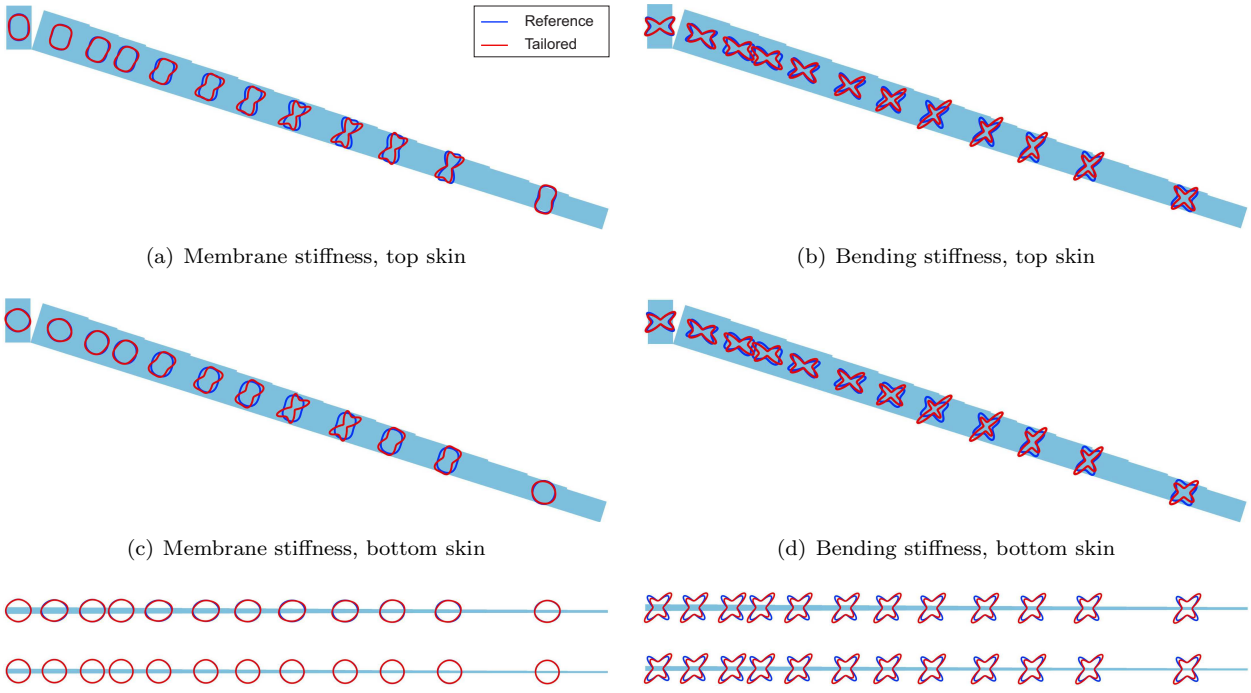


(a) Membrane stiffness, top skin

(b) Bending stiffness, top skin

(c) Membrane stiffness, bottom skin

(d) Bending stiffness, bottom skin

(e) Membrane stiffness, spars

(f) Bending stiffness, spars

**Figure 9. Comparison of composite tailoring between the reference wing and the tailored wing**

and local angle of attack distribution are presented and summarised in terms of cumulative root loads.

Comparison of the aeroelastic out-of-plane and torsional deformation between the two wing types for the selected load cases is shown in Fig. 10. One can observe that the tailored wing is considerably more flexible in comparison to the reference wing. The difference in the observed tip deflection is 46% for 1 g, 23% for 5 g, and 8% for −2 g load case. Relatively small difference in tip deflection in the case of the −2 g load case can be explained by considerably higher aerodynamic loads on the outboard part of the reference wing as shown in Fig. 13b. The difference in tip twist between the two wings is even larger. It amounts to 121%, 133%, and 140% for the 1 g, 5 g, and −2 g load case respectively. The difference is attributed to the overall thinner skins and the bend-twist coupling tailored into the laminates comprising the tailored wing wingbox.

Second important aspect of the structural part of the aeroelastic response are the buckling and strain constraints that were imposed on the wing design during the optimisation process. Figs. 11 and 12 show to what extent are the buckling and the strain constraints critical at the selected load cases for the reference wing and the tailored wing. Evidently, the buckling constraint is the more critical constraint of the two for both wing types. Most of the top and bottom skin is critical in buckling due to the high compressive loads present in the skins at the respective load cases of 5 g and −2 g. It is noteworthy that the critical value for buckling is 0.57 instead of one due to the application of the safety factor.

Despite relatively high out-of-plane deflection of about 10% at 5 g and the application of safety factor and material knock-downs, the strain constraint is not critical for neither of the two wings. In the case of the reference wing the strain coefficient does not exceed 0.25 anywhere on the wing, whereas in the case of the tailored wing, the maximum strain coefficient does not exceed the value of 0.4. It is noteworthy that the relatively high strain values in the tailored wing are confined to a narrow region in the mid section of the wing in the 5 g load case.

Finally, it is evident that the spars are not critical in neither buckling nor strain for any of the two wings. It was shown in the preceding section that spars thickness is governed by the minimum thickness constraint which was selected due to manufacturing reasons. Consequently, the spars are sufficiently strong to easily resists the buckling loads and strains.

Lift distribution for the reference and the tailored wing is compared in Fig. 13. First, both wings exhibit almost identical lift distribution at the 1 g load case, which results from enforcing the cruise shape in terms of wing twist as a design constraint. Second, there is a significant difference in lift distribution between the two

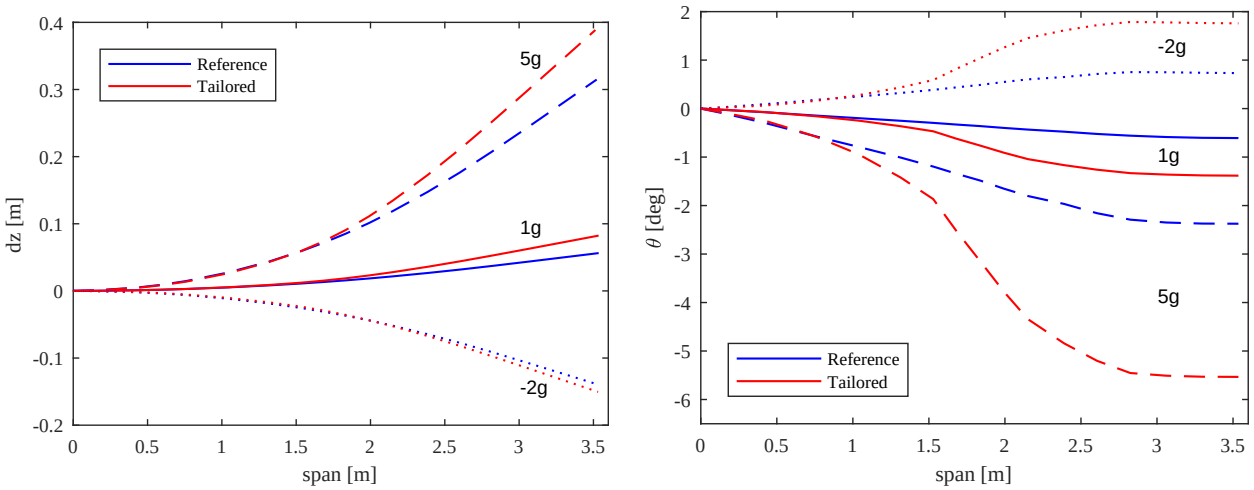


(a) Out-of-plane deformation

(b) Torsional deformation

**Figure 10. Aeroelastic deformation at the design load cases**

wings in the 5 g and −2 g load case due to higher bend-twist coupling present in the laminates comprising the tailored wing which allow the tailored wing to redistribute aerodynamic loads towards the root of the wing. The spanwise location of the centre of pressure for both wings is at 42.8% of the span in 1 g load case. At 5 g load case the spanwise location of the centre of pressure moves to 47.4% and to 44.5% of the span for the reference and the tailored wing respectively. Similarly, at −2 g load case the spanwise location of the centre of pressure for the reference wing moves to 51.2% of the span and to 45.6% of the span for the tailored wing. One can observe that there is a larger difference between the two wings in the case of the −2 g load case, which is explained by the difference in the jig shape of the two wings. As already mentioned, the reference wing requires considerably more wash-out built in the jig shape in order to satisfy the cruise shape constraint, which leads to increased outboard loading of the wing in the case of negative load cases. This is also confirmed by the comparison shown in Fig. 13b.

Local angle of attack comparison is shown in Fig. 14. Expectedly the two wings exhibit almost identical angle of attack distribution along the span for a 1 g load case. The 4% difference in structural mass between the two wings has a negligible effect on the angle of attack. Moreover, the local angle of attack indicates that both wings follow closely the required 1 g twist distribution, namely the local angle of attack should linearly decrease by 2 deg from root to tip.

The local angle of attack at 5 g and −2 g load case reflects the differences in torsional deformation observed between the two wings, which results in a larger absolute value of the local angle of attack at the root and a lower absolute value at the tip of the tailored wing relative to the reference wing. Such behaviour is typical for composite wings tailored for steady manoeuvre load alleviation.

It is noteworthy that the angle of attack at the root corresponds to the trim angle of attack for the whole aircraft. A trimmed flight condition (weight equals lift) is obtained at −0.30 deg angle of attack for both wings at the 1 g load case. Whereas at 5 g and −2 g load case, the reference wing is trimmed at 10.1 deg and −7.9 deg, and the tailored wing is trimmed at 10.9 deg and −8.6 deg respectively.

Finally, the root forces and moments for the two wing types are presented in Table 3. Expectedly, both wings exhibit almost identical shear force in lift direction, $V_z$, and the corresponding root bending moment, $M_x$, at 1 g load case which indicates that the cruise shape constraint was successfully imposed on both wings. There is a noticeable difference in shear force in spanwise direction, $V_y$, and the corresponding root bending moment, $M_z$ which is attributed to the difference in the out-of-plane deflection.

Inspecting the obtained loads for a 5 g load case one can observe a 6% and an 11% reduction of root bending moment $M_x$ and torsional moment $M_y$ of the tailored wing relative to the reference wing with the shear forces maintained at similar magnitudes. The reduction in both $M_x$ and $M_y$ is explained by the lift redistribution towards the inboard section of the wing as observed in the case of tailored wing in Fig. 13. Similar conclusions can be drawn also for the −2 g load case with the $M_x$ reduction of 11% and $M_y$ reduction of 35%.

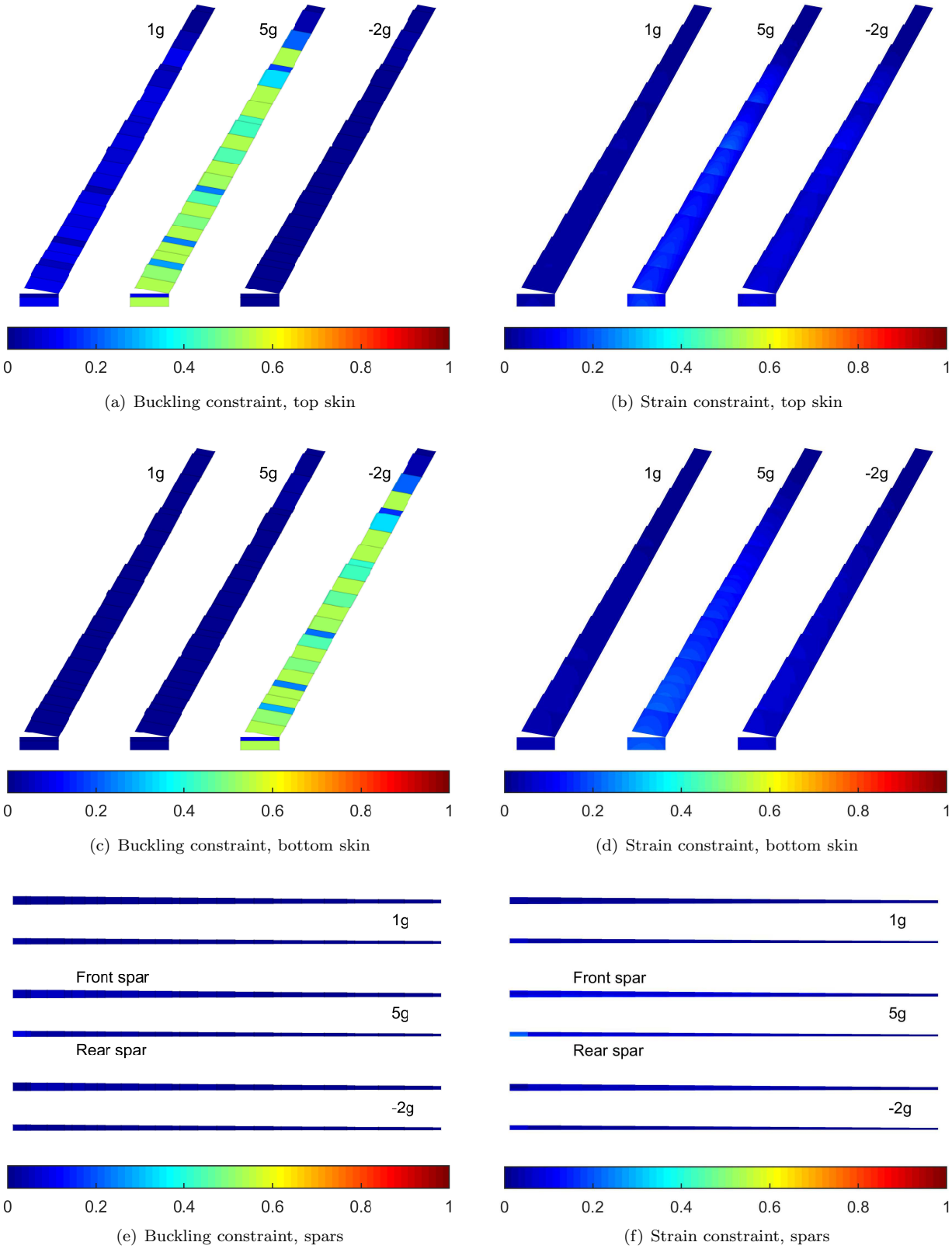


(a) Buckling constraint, top skin

(b) Strain constraint, top skin

(c) Buckling constraint, bottom skin

(d) Strain constraint, bottom skin

(e) Buckling constraint, spars

(f) Strain constraint, spars

**Figure 11. Comparison of buckling and strain design constraint for the reference wing**

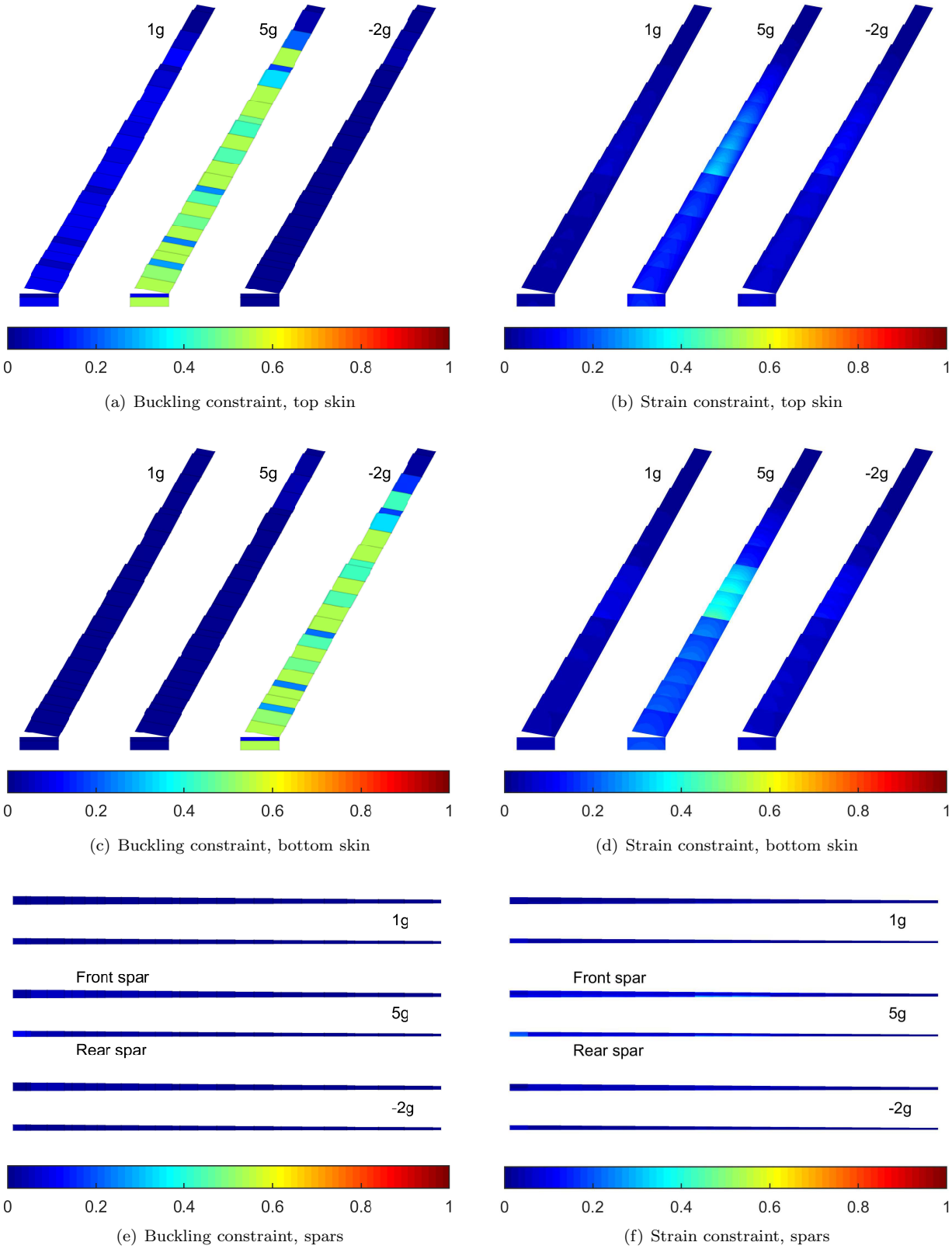


(a) Buckling constraint, top skin

(b) Strain constraint, top skin

(c) Buckling constraint, bottom skin

(d) Strain constraint, bottom skin

(e) Buckling constraint, spars

(f) Strain constraint, spars

**Figure 12. Comparison of buckling and strain design constraint for the tailored wing**

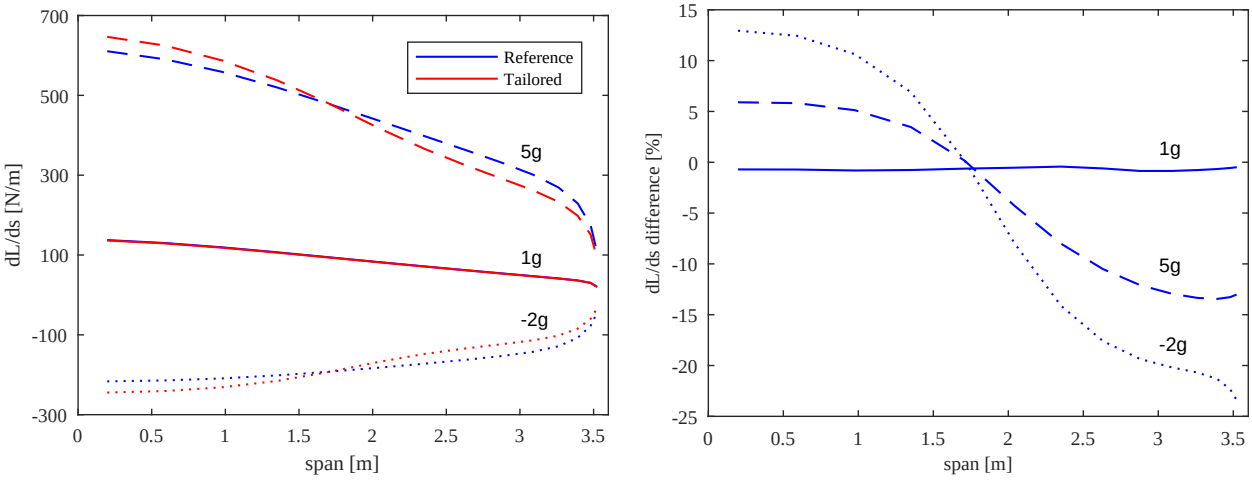


(a) Lift distribution (b) Comparison of the lift distribution

**Figure 13. Lift distribution at design load cases**

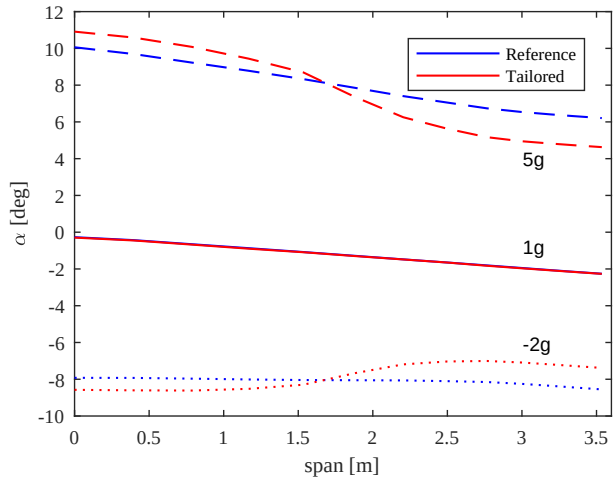


**Figure 14. Local angle of attack along the span in trimmed flight at design load cases**

**Table 3. Comparison of the root forces and moments**

| Wing | $V_x$ [N] | $V_y$ [N] | $V_z$ [N] | $M_x$ [Nm] | $M_y$ [Nm] | $M_z$ [Nm] |
|---|---|---|---|---|---|---|
| load case: 1g | | | | | | |
| Reference | 0.96 | -3.9 | 202.4 | 304 | -93.2 | -3.8 |
| Tailored | 1.04 (1.09)† | -5.6 (1.43) | 202.4 (1.00) | 305 (1.00) | -93.5 (1.00) | -5.1 (1.35) |
| load case: 5g | | | | | | |
| Reference | -176.8 | -25.5 | 996.4 | 1662 | -326.5 | 262.8 |
| Tailored | -191.5 (1.08) | -34.2 (1.34) | 993.7 (1.00) | 1555 (0.94) | -291.4 (0.89) | 257.5 (0.98) |
| load case: -2g | | | | | | |
| Reference | -55.8 | 6.7 | -400.9 | -726 | 76.9 | 98.4 |
| Tailored | -60.4 (1.08) | 10.5 (1.56) | -400.3 (1.00) | -647 (0.89) | 49.9 (0.65) | 95.1 (0.97) |

† relative to the reference wing (Tailored/Reference)

## VI. Conclusion

Aeroelastic framework developed at Delft University of Technology was successfully applied to a preliminary design of two aeroelastically tailored wings for a flying unmanned aerial vehicle demonstrator. The main difference between the two wings is in the laminate definition. The reference wing used symmetric-balanced laminate while the tailored wing used symmetric-only laminates. The selected design setup in terms of wing structural layout, load case, design objective, and constraint selection led to a wing design which was predominantly driven by the buckling and minimum thickness constraint. As a result the tailored wing was 4% lighter than the reference wing in terms of structural mass which translates to a 1% mass reduction for the whole aircraft. In addition to mass savings, the root bending moment of the tailored wing was reduced by 6% and 11% relative to the reference wing for the 5 g and −2 g load case.

Application of the cruise shape as a design constraint was successfully demonstrated. Resulting in a nearly identical aeroelastic response in terms of lift distribution, and local angle of attack in the 1 g load case. Within this scope the jig shape of both wings was also successfully retrieved. Significant differences were observed in the jig shapes of the two wings. Most importantly, the jig shape of the reference wing required significantly more pre-twist in comparison to the jig shape of the tailored wing. At the tip, the difference in pre-twist was more than 40%. The observed differences are attributed to the different laminate constraint used for the reference and the tailored wing.

The prescribed cruise shape was found to have an important effect on the ability of the reference wing to alleviate loads in the −2 g load case. The aerodynamic loads over the outboard half of the wing of the reference wing compared to the tailored wing were more than 30% higher for the −2 g load case relative to the loads obtained for the 5 g load case. The asymmetry in the aeroelastic response to positive and negative load cases reflected also in the final design of the reference wing. The relative thickness of the bottom skin of the reference wing in comparison to the tailored wing was 50% larger than the relative thickness of the top skin.

## Acknowledgements

The work presented herein has been partially funded by the European Community's Horizon 2020 Programme (H2020) under the Grant Agreement 636307. The FLEXOP project (Flutter Free FLight Envelope eXpansion for ecOnomical Performance improvement) is a project funded under the topic MG-1.1-2014. involving 10 partners. The project started on June 1st 2015.

## References

[1]Shirk, M. H., Hertz, T. J., and Weisshaar, T. A., "Aeroelastic tailoring - Theory, practice, and promise," *Journal of Aircraft*, Vol. 23, No. 1, jan 1986, pp. 6–18.

[2]Qin, Z., Marzocca, P., and Librescu, L., "Aeroelastic instability and response of advanced aircraft wings at subsonic flight speeds," *Aerospace Science and Technology*, Vol. 6, No. 3, mar 2002, pp. 195–208.

[3]Qin, Z., Librescu, L., and Marzocca, P., "Aeroelasticity of composite aerovehicle wings in supersonic flows," *Journal of spacecraft and rockets*, Vol. 40, No. 2, 2003, pp. 162–173.

[4]Weisshaar, T. A., "Aeroelastic tailoring - Creative uses of unusual materials," *28th Structures, Structural Dynamics and Materials Conference*, apr 1987.

[5]Danilin, A. and Weisshaar, T. A., "The Use of Optimality Criteria for Aircraft Conceptual Level Structural Design," *41st AIAA/ASME/ASCE/AHS Structural Dynamics and Materials Conference*, No. AIAA Paper 2000-1328, American Institute of Aeronautics and Astronautics, 2000.

[6]Livne, E. and Weisshaar, T. A., "Aeroelasticity of Nonconventional Airplane Configurations-Past and Future," *Journal of Aircraft*, Vol. 40, No. 6, 2003, pp. 1047–1065.

[7]Weisshaar, T. A. and Duke, D. K., "Induced Drag Reduction Using Aeroelastic Tailoring with Adaptive Control Surfaces," *Journal of Aircraft*, Vol. 43, No. 1, 2006, pp. 157–164.

[8]Eastep, F. E., Tischler, V. A., Venkayya, V. B., and Khot, N. S., "Aeroelastic Tailoring of Composite Structures," *Journal of Aircraft*, Vol. 36, No. 6, 1999, pp. 1041–1047.

[9]Arizono, H. and Isogai, K., "Application of Genetic Algorithm for Aeroelastic Tailoring of a {Cranked}-Arrow Wing," *Journal of Aircraft*, Vol. 42, No. 2, 2005, pp. 493–499.

[10]Guo, S. J., Bannerjee, J. R., and Cheung, C. W., "The effect of laminate lay-up on the flutter speed of composite wings," *Proceedings of the Institution of Mechanical Engineers, Part G: Journal of Aerospace Engineering*, Vol. 217, No. 3, 2003, pp. 115–122.

[11]Guo, S., Cheng, W., and Cui, D., "Optimization of Composite Wing Structures for Maximum Flutter Speed," *46th*

*AIAA/ASME/ASCE/AHS/ASC Structures, Structural Dynamics and Materials Conference*, Vol. 6, American Institute of Aeronautics and Astronautics, Reston, Virigina, apr 2005, pp. 1–10.

[12]Dillinger, J. K. S., Abdalla, M. M., Klimmek, T., and Gürdal, Z., "Static aeroelastic stiffness optimization and investigation of forward swept composite wings," *10th World Congress on Structural and Multidisciplinary Optimization*, Orlando, Florida, USA, 2013.

[13]Guo, S. J., Cheng, W., and Cui, D., "Aeroelastic tailoring of composite wing structures by laminate layup optimization," *AIAA Journal*, Vol. 44, No. 12, 2006, pp. 3146–3150.

[14]Kameyama, M. and Fukunaga, H., "Optimum design of composite plate wings for aeroelastic characteristics using lamination parameters," *Computers and Structures*, Vol. 85, No. 3-4, 2007, pp. 213–224.

[15]Manan, A., Vio, G. A., Harmin, M. Y., and Cooper, J. E., "Optimization of aeroelastic composite structures using evolutionary algorithms," *Engineering Optimization*, Vol. 42, No. 2, 2010, pp. 171–184.

[16]De Leon, D. M., De Souza, C. E., Fonseca, J. S. O., and Da Silva, R. G. A., "Aeroelastic tailoring using fiber orientation and topology optimization," *Structural and Multidisciplinary Optimization*, Vol. 46, No. 5, 2012, pp. 663–677.

[17]Pettit, C. L. and Grandhi, R. V., "Optimization of a wing structure for gust response and aileron effectiveness," *Journal of Aircraft*, Vol. 40, No. 6, 2003, pp. 1185–1191.

[18]Kim, T. U. and Hwang, I. H., "Optimal design of composite wing subjected to gust loads," *Computers and Structures*, Vol. 83, No. 19-20, 2005, pp. 1546–1554.

[19]Stodieck, O., Cooper, J. E., Weaver, P. M., and Kealy, P., "Improved aeroelastic tailoring using tow-steered composites," *Composite Structures*, Vol. 106, 2013, pp. 703–715.

[20]Thuwis, G. A. A., De Breuker, R., Abdalla, M. M., and Gürdal, Z., "Aeroelastic tailoring using lamination parameters: Drag reduction of a Formula One rear wing," *Structural and Multidisciplinary Optimization*, Vol. 41, No. 4, 2010, pp. 637–646.

[21]Sherrer, V. C., Hertz, T. J., and Shirk, M. H., "Wind Tunnel Demonstration of Aeroelastic Tailoring Applied to Forward Swept Wings," *Journal of Aircraft*, Vol. 18, No. 11, nov 1981, pp. 976–983.

[22]Blair, M. and Weisshaar, T. A., "Swept composite wing aeroelastic divergence experiments," *Journal of Aircraft*, Vol. 19, No. 11, nov 1982, pp. 1019–1024.

[23]Hollowell, S. J. and Dugundji, J., "Aeroelastic flutter and divergence of stiffness coupled, graphite/epoxy cantilevered plates," *Journal of Aircraft*, Vol. 21, No. 1, jan 1984, pp. 69–76.

[24]Landsberger, B. J. and Dugundji, J., "Experimental aeroelastic behavior of unswept and forward-swept cantilever graphite/epoxy wings," *Journal of Aircraft*, Vol. 22, No. 8, aug 1985, pp. 679–686.

[25]Chen, G.-S. and Dugundji, J., "Experimental aeroelastic behavior of forward-swept graphite/epoxy wings with rigid-body freedom," *Journal of Aircraft*, Vol. 24, No. 7, jul 1987, pp. 454–462.

[26]Werter, N. P. M., Sodja, J., and De Breuker, R., "Design and Testing of Aeroelastically Tailored Wings Under Maneuver Loading," *AIAA Journal*, Vol. 55, No. 3, 2017, pp. 1012–1025.

[27]Sodja, J., Werter, N. P. M., Dillinger, J. K. S., and De Breuker, R., "Dynamic Response of Aeroelastically Tailored Composite Wing: Analysis and Experiment," *57th AIAA/ASCE/AHS/ASC Structures, Structural Dynamics, and Materials Conference*, 2016.

[28]"A novel dynamic aeroelastic framework for aeroelastic tailoring and structural optimisation," *Composite Structures*, Vol. 158, dec 2016, pp. 369–386.

[29]Ferede, E. and Abdalla, M., "Cross-sectional modelling of thin-walled composite beams," *55th AIAA/ASME/ASCE/AHS/ASC Structures, Structural Dynamics, and Materials Conference*, American Institute of Aeronautics and Astronautics, Reston, Virginia, jan 2014.

[30]Werter, N. P. M., De Breuker, R., and Abdalla, M. M., "Continuous-Time State-Space Unsteady Aerodynamic Modeling for Efficient Loads Analysis," *AIAA Journal*, , No. Dlm, 2017, pp. 1–12.

[31]De Breuker, R., Abdalla, M. M., and Gürdal, Z., "Design of morphing winglets with the inclusion of nonlinear aeroelastic effects," *Aeronautical Journal*, Vol. 115, No. 1174, 2011, pp. 713–728.

[32]Werter, N., De Breuker, R., Beaverstock, C. S., Friswell, M., and Dettmer, W., "Two-level Conceptual Design of Morphing Wings," apr 2013.

[33]Werter, N., *Aeroelastic Modelling and Design of Aeroelastically Tailored and Morphing Wings*, Phd thesis, Delft University of Technology, 2017.

[34]Kassapoglou, C., *Design and Analysis of Composite Structures*, John Wiley & Sons Ltd, Oxford, UK, may 2013.